# Quantitative in vivo assessment of human mitral valve coaptation area after undersized ring annuloplasty repair for ischemic mitral regurgitation



Natalie T. Simonian, BS,[a] Hao Liu, PhD,[a] Alison M. Pouch, PhD,[b] Joseph H. Gorman III, MD,[c] Robert C. Gorman, MD,[c] and Michael S. Sacks, PhD[a]

## ABSTRACT

**Objectives:** Long-term outcomes of mitral valve repair procedures to correct ischemic mitral regurgitation remain unpredictable, due to an incomplete understanding of the disease process and the inability to reliably quantify the coaptation zone using echocardiography. Our objective was to quantify patient-specific mitral valve coaptation behavior from clinical echocardiographic images obtained before and after repair to assess coaptation restoration and its relationship with long-term repair durability.

**Methods:** To circumvent the limitations of clinical imaging, we applied a simulation-based shape-matching technique that allowed high-fidelity reconstructions of the complete mitral valve in the systolic configuration. We then applied this method to an extant database of human regurgitant mitral valves before and after undersized ring annuloplasty to quantify the effect of the repair on mitral valve coaptation geometry.

**Results:** Our method was able to successfully resolve the coaptation zone into distinct contacting and redundant regions. Results indicated that in patients whose regurgitation recurred 6 months postrepair, both the contacting and redundant regions were *larger* immediately postrepair compared with patients with no recurrence ($P < .05$), even when normalized to account for generally larger recurrent valves.

**Conclusions:** Although increasing leaflet coaptation area is an intuitively obvious way to improve long-term repair durability, this study has implied that this may not be a reliable target for mitral valve repair. This study underscores the importance of a rigorous understanding of the consequences of repair techniques on mitral valve behavior, as well as a patient-specific approach to ischemic mitral regurgitation treatment within the context of mitral valve and left ventricle function. (JTCVS Techniques 2022;16:49-59)

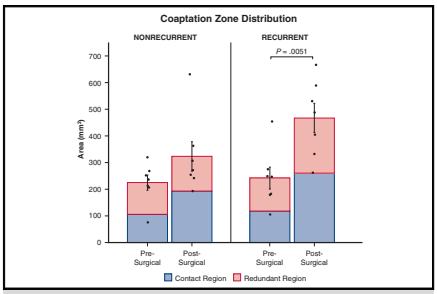


**The coaptation zone is *larger* in patients with recurrence after URA.**

### CENTRAL MESSAGE

Increased MV leaflet coaptation area alone may not be a reliable target for long-term durability in MV repair of IMR.

### PERSPECTIVE

Patient outcomes of regurgitant MV repair remain unpredictable, due to an incomplete understanding of repair complexities and limitations of echocardiographic imaging. We applied an image-based simulation technique to quantify the coaptation zone in repaired MVs and demonstrated that increased coaptation may not be a reliable target for long-term repair durability.

▶ Video clip is available online.

Undersized ring annuloplasty (URA) is currently the gold standard for mitral valve (MV) repair in ischemic mitral regurgitation (IMR).[1] However, 6 months after URA repair, up to 30% of patients with IMR experience recurrent regurgitation,[2] and long-term outcomes remain unpredictable, suboptimal, and poorly understood.[3-9] Thus, there is an urgent need for a deeper, quantitative understanding of the functional consequences of MV repair to develop more durable mitral regurgitation (MR) treatments.

From the [a]James T. Willerson Center for Cardiovascular Modeling and Simulation, The Oden Institute for Computational Engineering and Sciences and the Department of Biomedical Engineering, The University of Texas at Austin, Austin, Tex; [b]Departments of Radiology and Bioengineering, University of Pennsylvania, Philadelphia, Pa; and [c]Department of Surgery, Smilow Center for Translational Research, Gorman Cardiovascular Research Group, Perelman School of Medicine, University of Pennsylvania, Philadelphia, Pa.

This work was supported by the National Heart, Lung, and Blood Institute of the National Institutes of Health (R01HL073021 to M.S.S. and R.C.G. and R01 103723 to M.S.S. and R.C.G.) and the Moss Foundation.

Received for publication June 8, 2022; revisions received Aug 29, 2022; accepted for publication Sept 13, 2022; available ahead of print Oct 1, 2022.

Address for reprints: Michael S. Sacks, PhD, Department of Biomedical Engineering, The Oden Institute for Computational Engineering and Sciences, The University of Texas at Austin, 201 East 24th St, Stop C0200, Austin, TX 78712-1229 (E-mail: msacks@oden.utexas.edu).

2666-2507



https://doi.org/10.1016/j.xjtc.2022.09.013

**Abbreviations and Acronyms**

CMF = chordal mimicking force
ED = end-diastolic
ES = end-systolic
FE = finite element
IMR = ischemic mitral regurgitation
LV = left ventricle
MR = mitral regurgitation
MV = mitral valve
MVTa = mitral valve tenting area
rt-3DE = real-time 3-dimensional echocardiography
URA = undersized ring annuloplasty

Given that poor coaptation is the underlying mechanistic driver of MR, restoring normal coaptation would seem to be a critical objective in MV repair. Intuitively, it would seem that a larger coaptation area signifies better closure and therefore a more durable repair, a syllogism that constitutes one of Carpentier's 3 guiding principles of reconstructive MV surgery.[1,10] However, intraoperative assessment of coaptation pre- or postrepair is inhibited by the poor spatial resolution of real-time 3-dimensional echocardiography (rt-3DE) imaging.[11] Furthermore, in the limited area that is visible, it is currently not possible to distinguish the 2 leaflets or to resolve any further detail. Consequently, existing methods to compute coaptation area are restricted to indirect calculations using comparative measurements of full and uncoapted leaflet length at diastole and systole, respectively,[12-15] or underestimate the true area by measuring only what is directly visible in rt-3DE images.[16,17] Current intraoperative methods for assessing coaptation rely mainly on a measurement of coaptation length of at least 8 mm from rt-3DE imaging, which not only can be underestimated but also represents a simplistic 1-dimensional geometric assessment of the complex coaptation behavior of the MV.[6,18-20] Clearly, there is a need for a precise quantification of coaptation behavior using readily available clinical imaging data.

In the present study, we quantified the full 3-dimensional MV coaptation zone geometry before and after URA repair of MVs with IMR using clinically obtained rt-3DE images using our MV shape-matching approach.[21] This technique allowed us to fully resolve the MV coaptation zone into its contacting and redundant subregions. We then analyzed the functional impact of the repair at a level of detail not previously investigated, providing for a more nuanced understanding of the closing behavior of the regurgitant MV.

## MATERIALS AND METHODS

### Overview of the Approach

An extant database of rt-3DE images of MVs of 14 patients with IMR from a previous study on MV strain before and after URA repair were analyzed.[22,23] First, the images were segmented and processed, and the subsequent meshes were used as the inputs for our finite element (FE)-based closure simulation. In this simulation, the MV is initially closed by applying physiological loading and boundary conditions. Subsequently, a local corrective pressure field is applied to correct for shape mismatch and ensure the final shape of the MV closely corresponds to its true shape as segmented from the rt-3DE image. Extensive validation of this method confirms that this technique results in an accurate representation of the true, end-systolic (ES) state MV, which is a significant improvement over the visualization limits of modern rt-3DE imaging. From this final closed mesh, the coaptation zone is subdivided into the contacting and redundant regions, and the areas of the leaflets and coaptation regions are computed and compared to better understand the impact of the ring implant on MV coaptation.

### Shape-Matching Closure Simulation

**Imaging.** Rt-3DE imaging was performed according to a previously described protocol[23] immediately before and after URA repair in 14 patients with grade 3 or 4 IMR at the time of surgery. Each dataset captured 2 to 3 consecutive cardiac cycles with 6 to 12 frames per cycle at a voxel resolution of 0.6 to 0.8 mm. Seven of the 14 patients had no recurrence of IMR 6 months postrepair, whereas the remaining 7 patients demonstrated recurrent IMR of grade 2 or higher at the same time point. Of the available data, only images with fully visible MV leaflets were used in this study. In the previous study from which these images were obtained, approval was granted by the Institutional Review Boards of the University of Pennsylvania, University of Pittsburgh, and Beth Israel Deaconess Medical Center, and written informed consent was obtained from all patients.[23]

**Finite element–based shape–matching method for planar strain estimation.** The methods for this technique to estimate MV leaflet strain from rt-3DE images of patient MVs has been extensively detailed in prior publications.[21,22] From the rt-3DE data series acquired of each patient's MV immediately before and after URA repair, representative images in the open (end-diastolic [ED]) and closed (ES) states were used to develop 3-dimensional shell representations of each geometry in a MATLAB-based tracing and meshing pipeline (Figure 1). To build direct material correspondence between the ED and ES states and to completely reconstruct the coaptation zone, we morphed the open state MV mesh to its corresponding closed shape using an FE-based closure simulation (Figure 2). Our FE-based shape morphing technique has been previously described and extensively validated using both high-fidelity micro computed tomography data and in vivo strain measurements. In both cases, the shape-morphing technique was able to reproduce the local strain field with excellent agreement to the in vitro and in vivo data and enforce the true closed shape of the MV as segmented from rt-3DE to within a signed intersurface distance of $0.035 \pm 0.223mm$.[21] All shape-matching simulations were performed using the commercial FE software package Abaqus 6.13 (SIMULIA, Dassault Systèmes, Providence, Rhode Island).

### Computing the Coaptation Area

The coaptation zone of the MV was subdivided into the contact area (the region where the 2 leaflets are in direct contact) and the redundant region (the portion of the leaflet which hangs below the free edge of the opposing leaflet) (Figure 3, *B*). Contacting elements are defined as those with centroids within 0.8 mm (the voxel resolution) of each other, and with nearly antiparallel outward normals $n_a$ and $n_b$ for each respective element $a$ and $b$, such that $n_a \cdot n_b \leq -0.98$ (Figure 3, *C*). Redundant region elements were selected manually in ParaView (Kitware Inc) by visualizing the valve from the positive and negative $y$ axes and extracting all elements that were visible below the free edge of the other leaflet. Any elements that were identified as both contact and redundant were assigned to the contact set. To determine which elements corresponded to the anterior and posterior leaflets, the outward normal of each element was dotted with the

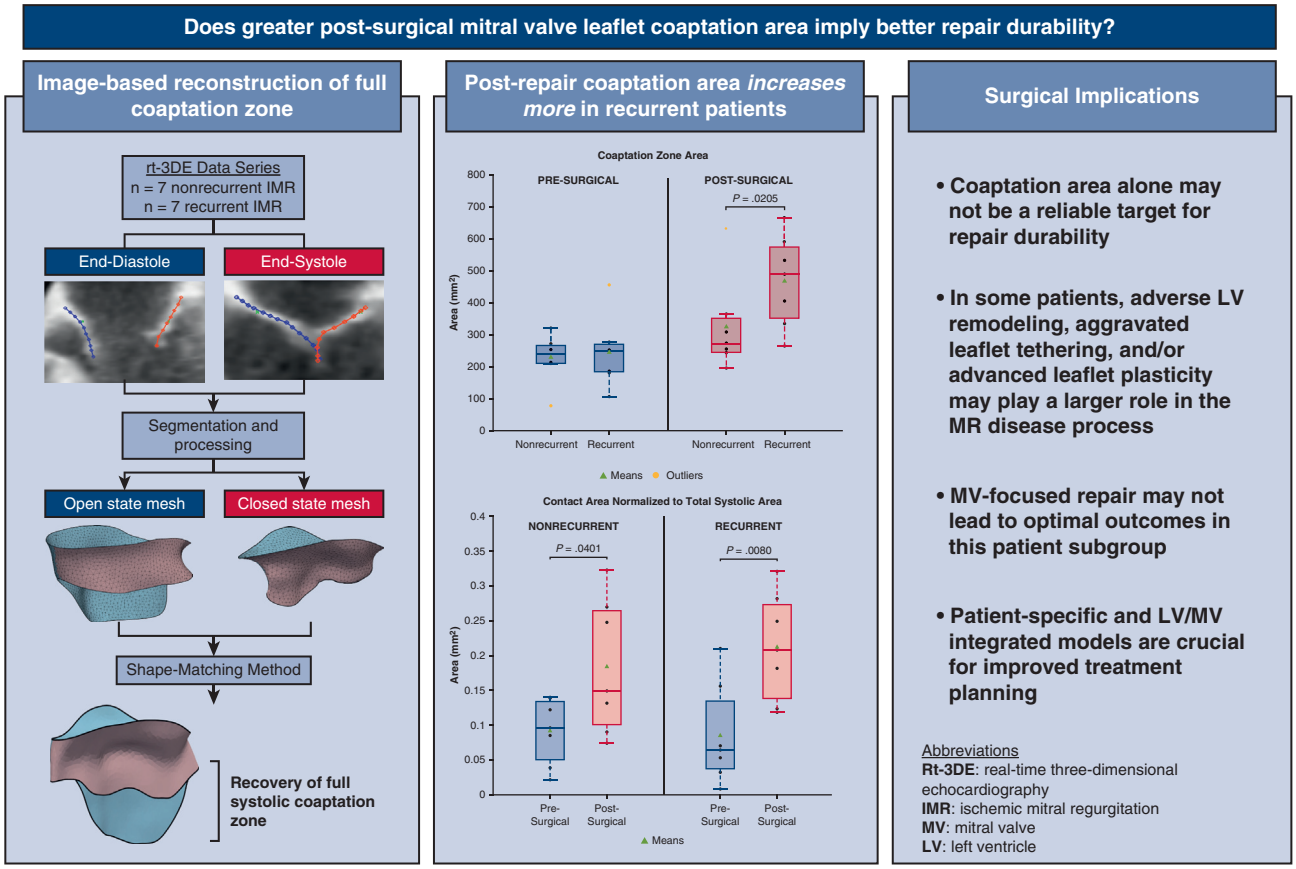


**FIGURE 1.** A noninvasive simulation-based method was used to quantify the coaptation zone area from rt-3DE images. Results demonstrated that post-surgical coaptation zone area was *greater* in patients with recurrent IMR at 6 months compared with patients without recurrence ($P < .05$). The contacting region area (where the 2 leaflets are in direct contact) was also *greater* in patients with recurrence, even when normalized to total systolic leaflet area to account for generally larger recurrent MVs. *rt-3DE*, Real-time 3-dimensional echocardiography; *IMR*, ischemic mitral regurgitation; *MR*, mitral regurgitation; *LV*, left ventricle; *MV*, mitral valve.

unit *y*-normal vector; a positive dot product defined the anterior leaflet, and a negative dot product defined the posterior leaflet. Finally, the areas of the elements in each set were calculated and summed to compute the total area of that region.

## Computing the MV Tenting Area

Central cross-sections (at x = 0) were obtained for all 14 patients from the ES shape-matched geometries, and the mitral valve tenting area (MVTa) was computed by tracing the leaflets until the line of contact and calculating the area of the enclosed boundary. To calculate the 2-dimensional annular area, principal component analysis was used to align the annulus to the Cartesian coordinate system, and then the annulus was projected onto the z-plane and its enclosed area computed.

## Statistical Analysis

To quantitatively assess differences between groups of MVs, we performed 1-tailed Student *t* tests to compare the areas of the various coaptation zone regions across the nonrecurrent and recurrent groups, as well as the tenting area. Given that the presurgical and postsurgical MVs are repeated measures, we used paired 1-tailed Student *t* tests to analyze the change in area.

## Validation

The shape-matching method has been carefully validated in previous work,[21] but in this study, special attention was paid to the recovery of the coaptation zone shape. Given that the shape-matching method works by morphing the simulated mesh to the target geometry segmented directly from rt-3DE, we aimed to demonstrate that the technique can recover the coaptation zone even without having a complete ES leaflet geometry to match, as limited in practice by ultrasound imaging. We used a previously extant set of 5 in vitro ovine MV meshes as the target geometries for the shape matching. Briefly, freshly explanted ovine MVs were instrumented with approximately 100 fiducial markers uniformly distributed over the full MV surface area and installed into a pulsatile flow loop to mimic a healthy left ventricle (LV).[24] The MVs were then imaged using a micro computed tomography scanner in both the ED (unloaded) and ES (fully loaded) states. These data were processed to reconstruct the ED leaflet geometry, and the ES leaflet geometry was reconstructed by iteratively building correspondence between the fiducial markers in the 2 states within a hyperelastic FE framework.

These segmentations were used as the input for the shape-matching simulation. First, we morphed the ED leaflet geometry to the ES leaflet geometry using the shape-matching technique and calculated the contact

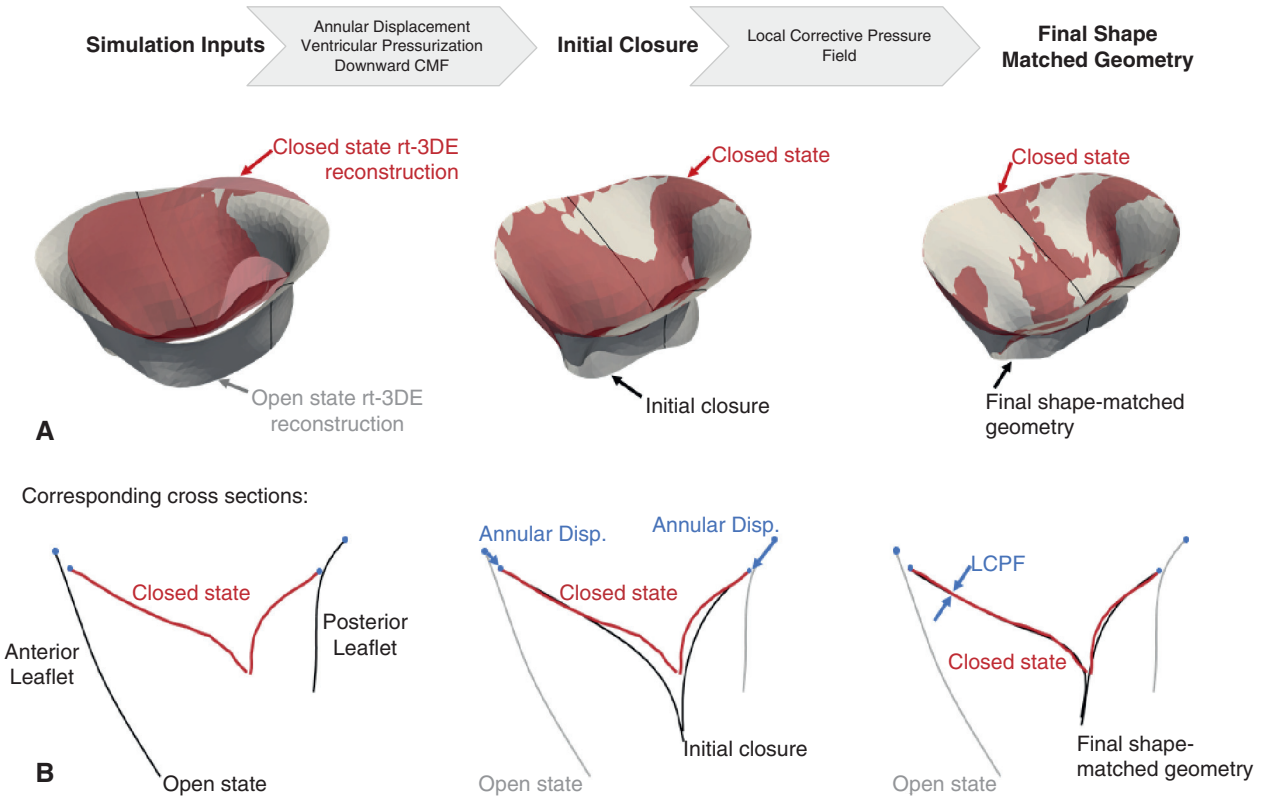


**FIGURE 2.** The progression of the FE closure simulation from the open state to the final, shape-matched closed state. A, The 3-dimensional meshes showing the simulated geometry (*grey*) and true, imaged closed state geometry (*red*) at the beginning of the simulation; after the initial FE closure with an annular displacement boundary condition and physiological ventricular pressurization and downward CMF as loading conditions; and after applying the LCPF to enforce the true imaged shape. B, The central cross-sections corresponding to the 3D meshes in (A) showing the simulated geometry and the true imaged closed state geometry at the same time points. *Red*: central cross-section of the true, imaged closed state leaflet medial surface. *Grey*: central cross section of the open segmented geometry of the MV, which is the input to the simulation. *Black*: central cross-section of the simulated geometry. *CMF*, chordal mimicking force; *rt-3DE*, real-time 3-dimensional echocardiography; *LCPF*, local corrective pressure field.

region area and redundant region area as described in Section Computing the Coaptation Area. To mimic the incomplete coaptation zone as visualized on echocardiography, we trimmed the coaptation zone at the coaptation line in ParaView (Kitware Inc) to produce the incomplete target geometry (Figure 4, *A*). Then, we similarly morphed the ED leaflet geometry to this incomplete target using shape-matching and recalculated the contact and redundant region areas (Figure 4, *B*). The values computed from the simulations with and without a full coaptation zone were compared using 1-tailed Student *t* tests.

## RESULTS

### Coaptation Zone Recovery

The shape-matching technique was able to fully recover the coaptation zone, which normally is not visible in part or in full on ultrasound (Figure 5, *A*, Video Abstract). Furthermore, this method differentiates the coaptation zone into its subdivisions, which is an as yet unprecedented level of geometric detail derived from rt-3DE images (Figure 5, *B*). This more precise insight into the closing behavior of the MV in both the diseased state and after URA repair will deepen our understanding of the impact of the ring on the MV and may help contextualize the divergent clinical outcomes among the patient groups.

### Human Undersized Annuloplasty Ring Repair

Overall, we observed that after repair, recurrent MVs had larger coaptation area and increased contact area compared with nonrecurrent valves (Figure 6, *B*; $P < .05$). In this same group, the redundant region also increased after repair (Figure 6, *C*; $P < .05$). Additionally, we noted that in all the MVs before and after repair, the majority of the redundant region is in the anterior leaflet (Figure 6, *C*).

Total systolic leaflet surface area decreased after surgical repair in both the nonrecurrent and recurrent valves (Figure 6, *A*; $P < .05$). Contact area increased more postsurgically in the recurrent group ($P = .0203$, $P > .05$ for nonrecurrent), a trend that holds even when normalized to total systolic leaflet area to account for generally larger recurrent valves (Figure 7, *A*; $P = .0080$, recurrent; $P = .0401$, nonrecurrent). The redundant region also increased postsurgically in recurrent valves ($P = .0050$, recurrent; $P > .05$,

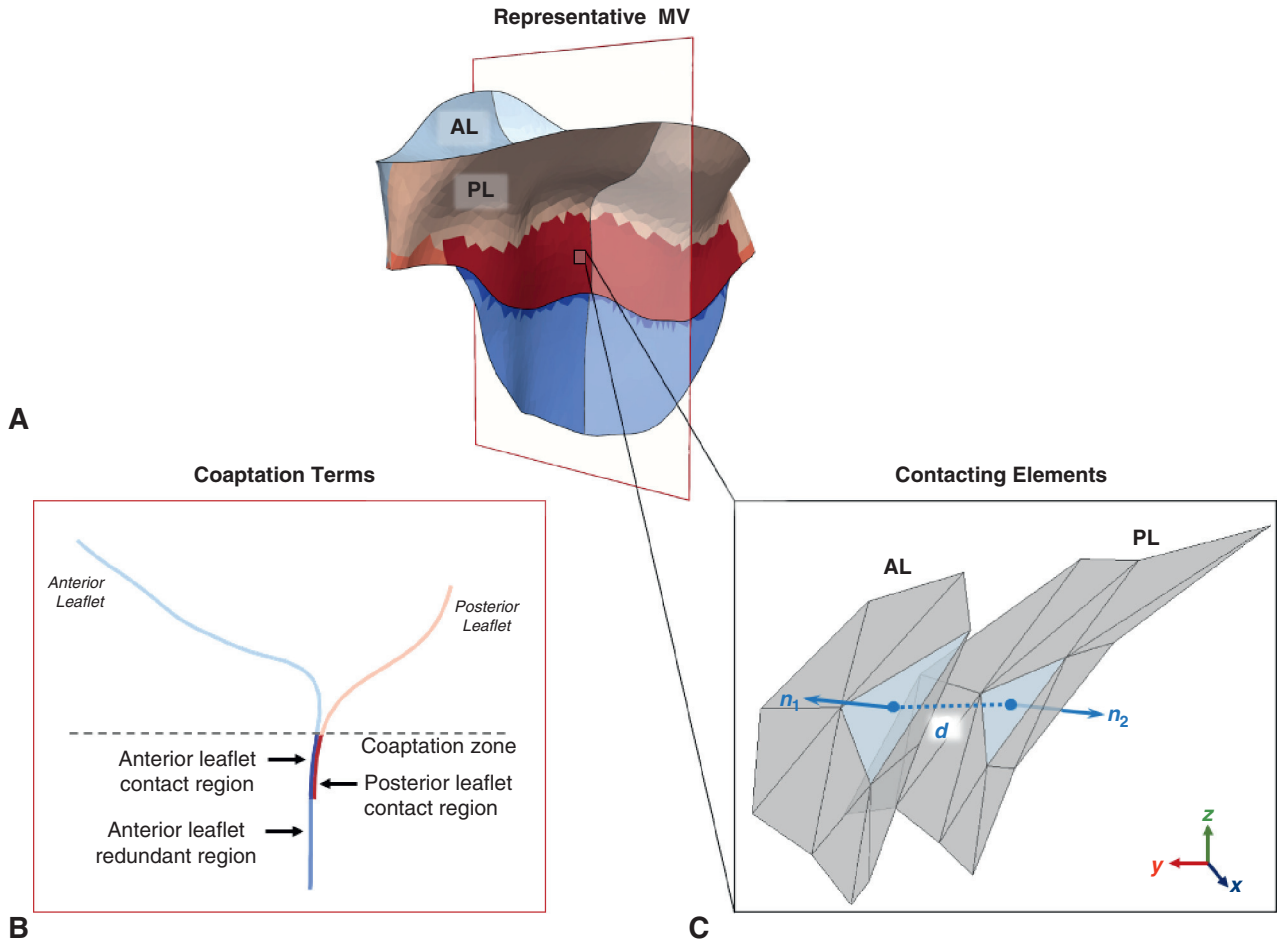


**FIGURE 3.** A, A representative MV with the coaptation sub-regions colored. B, A cross-section of the representative MV illustrating the 2 leaflets and the contact region, where the leaflets are physically in contact, and the redundant region, where tissue from 1 leaflet extends past the free edge of the opposing leaflet. C, An example of 2 contacting elements (*highlighted in blue*). The distance between the 2 centroids is at most 0.8 mm, and the dot product of their outward normal vectors is less than or equal to –0.98, indicating nearly antiparallel elements. *MV*, Mitral valve; *AL*, anterior leaflet; *PL*, posterior leaflet.

nonrecurrent), and again when normalized (Figure 7, *B*; $P = .0022$, recurrent; $P > .05$, nonrecurrent). A general increase in contact area is expected in the context of URA repair, whose aim is to force increased coaptation by decreasing the size of the annulus and thus better approximating the leaflets. However, it is important to note that contrary to expectations, MVs *with recurrence* of IMR at 6 months have *greater* normalized contact immediately after repair. Therefore, improved contact may not be a reliable metric for determining durability of the repair.

Although presurgical recurrent MVTa was significantly higher than nonrecurrent MVTa ($P < .05$), when normalized to measures of MV size using annular area or total systolic leaflet area, there was no longer a significant difference. After URA repair, there was no significant difference in absolute or normalized MVTa between the 2 groups (Table 1). This result suggests that MVTa was proportionally similar in both groups.

### Validation With In Vitro Fiducially Marked Ovine Mitral Valves

We observed no significant distortion in geometry when shape matching to the full target compared to the clipped target geometry. This consistency is a direct consequence of the hyperelastic FE framework that we used to regularize the shape-matching simulation. The minimum impact on geometry was confirmed by computing and comparing the contact and redundant region areas between the final simulated geometries when shape matching to a complete or incomplete target. We found no significant difference between these 2 metrics ($P > .1$ for both the contact and redundant region areas) (Figure 4, *B*). These results demonstrate

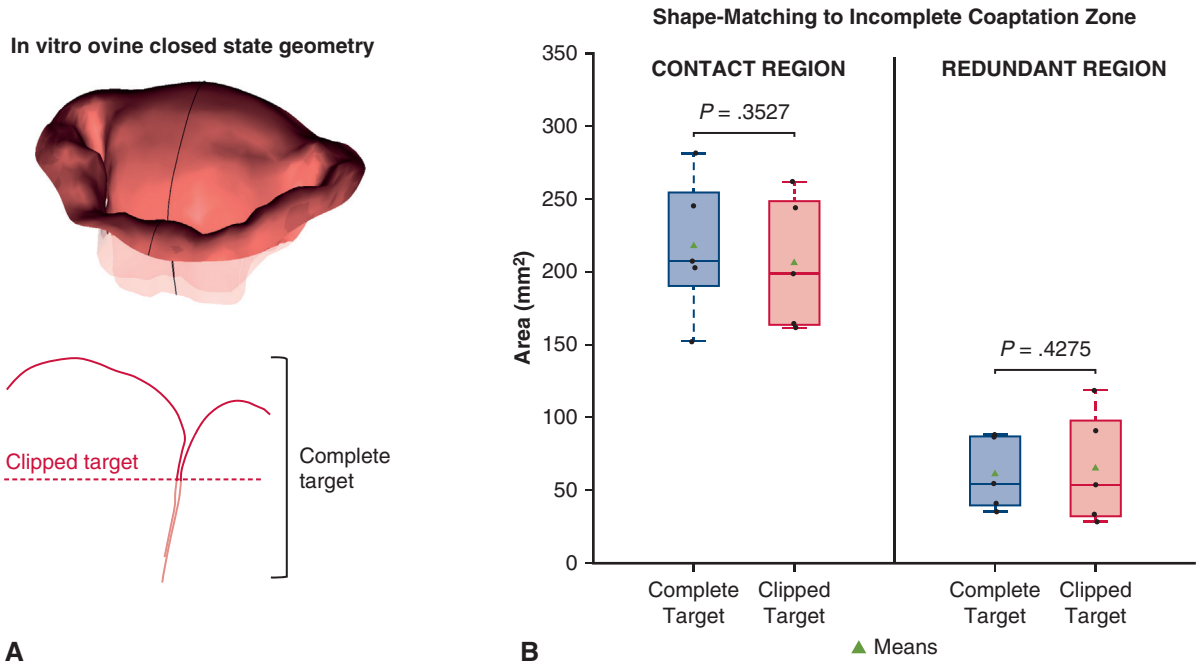


**FIGURE 4.** A, The full target closed geometry of a representative MV, and a cross-section showing the clipped target, which excludes the coaptation zone. B, The contact and redundant region areas were calculated from the final simulated geometries matched to targets with and without the full coaptation zone, and there was no significant difference between the measures.

that the shape-matching technique reliably reconstructed the MV coaptation zone even when the coaptation zone is incomplete or missing, which is a major limitation of echocardiographic imaging.

## DISCUSSION

### Overall Findings

Given that the fundamental functional basis of MV regurgitation is insufficient leaflet coaptation, one of Carpentier's guiding principles for MV repair is that increasing coaptation area leads to a more durable repair.[10] However, despite advances in annuloplasty and other repair techniques that aim to improve leaflet coaptation, recurrent MR continues to persist as a major clinical challenge in MR treatment.[16,23,25] Furthermore, although real-time echocardiography is a standard clinical tool in assessing MV function, a significant limitation of this imaging modality is that it cannot entirely resolve the crucial coaptation zone in the systolic position. Therefore, we aimed to reconstruct the coaptation zone using our state-of-the-art shape-matching technique, then to directly compute the associated areas at a high level of detail before and after surgical URA repair.

We found paradoxically that in patients who develop recurrent IMR 6 months after URA repair, the contact area immediately after repair was *greater* than that of patients who did not have recurrent MR at 6 months (Figure 6, *B*). Moreover, when normalized to total systolic leaflet area to account for generally larger presurgical MVs in the recurrent group, the contact area increased more in the recurrent group compared with the nonrecurrent group (Figure 7, *A*). The redundant region is also significantly greater in patients with recurrence, even when normalized (Figure 7, *B*).

These observations can be explained by the fact that all patients received approximately the same-sized annuloplasty ring. As the recurrent MVs had significantly larger prerepair annuli compared with the nonrecurrent MVs, using the similarly sized rings resulted in similar postsurgical annular orifice areas for both groups.[22] Therefore, recurrent MVs experienced a greater percent change in annulus reduction postrepair. Consequently, the recurrent MVs are likely more tethered after repair than their nonrecurrent counterparts, which may explain the suboptimal long-term outcomes for this group. Moreover, for the recurrent MVs, more leaflet tissue was shunted into the coaptation zone, increasing both contact and redundant region area for this subset. This shunting of tissue into the coaptation zone may also explain why total systolic leaflet area decreases after URA repair in both nonrecurrent and recurrent MVs (Figure 6, *A*). LV pressurization acts normal to the MV leaflet surface, and in the systolic position, pressurization in the coaptation zone of 1 leaflet is directly counterbalanced by equal and opposite pressurization on the other leaflet. Consequently, only leaflet tissue outside the coaptation zone can be deformed (ie, stretched) by LV pressurization. After URA repair, as more leaflet tissue is shunted into the

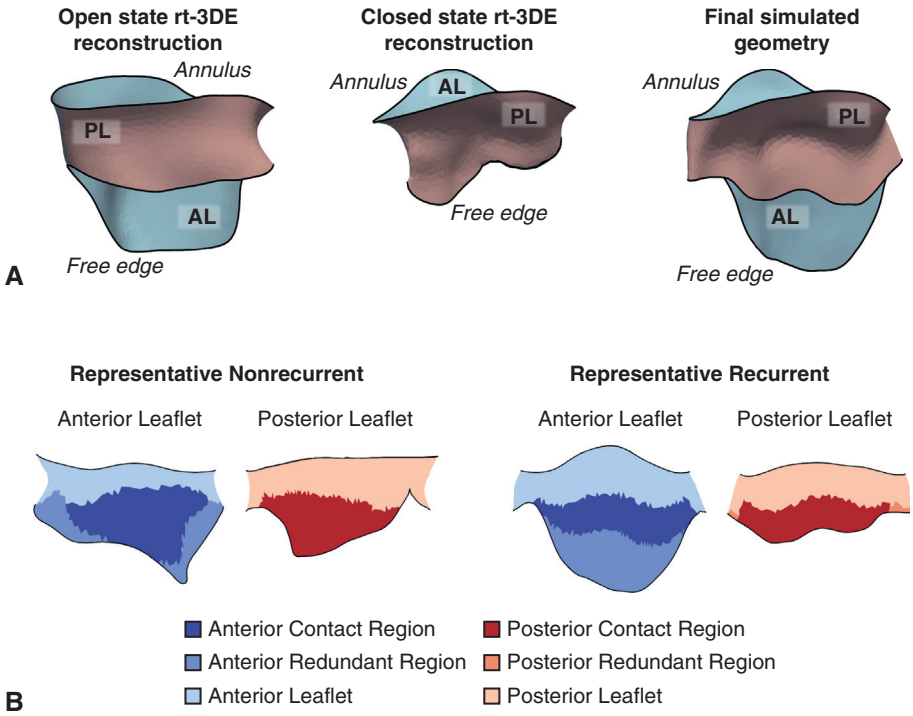


**FIGURE 5.** A, The open and closed geometries, as well as the simulation output, for a representative recurrent valve. The simulation is able to recover a large portion of the coaptation zone, which is not visible on the rt-3DE image but can be reconstructed from the fully visible open leaflet geometry. B, A representative nonrecurrent and recurrent MV after URA repair shown 2-dimensionally, with the elements of each coaptation region highlighted. *rt-3DE*, Real-time 3-dimensional echocardiography; *AL*, anterior leaflet; *PL*, posterior leaflet.

coaptation zone, there is less available deformable leaflet tissue compared to the presurgical state, and thus, the total systolic leaflet surface area decreases.

Furthermore, our analysis of the MVTa demonstrated that although there is a significant difference in measured values between presurgical nonrecurrent and recurrent ES MVTa, this difference disappears when MVTa were normalized to measures of MV size (Table 1). As a larger MV can be related to more advanced LV dilatation or simply larger patient size, MVTa may not necessarily reflect a more severe presentation of IMR. Although several studies have pointed to MVTa as a prognostic factor of clinical outcome, a study analyzing annular anteroposterior diameter-indexed MVTa in functional MR patients undergoing URA repair showed only a tendency toward prediction of clinical outcome.[26] Therefore, these results and those regarding the coaptation zone suggest that MV geometric indices may be insufficient to reliably assess the complex kinematic sequelae of IMR that crucially influence repair outcomes.

In addition, we have also demonstrated in this study the utility of our shape-matching technique in recovering the full coaptation zone, which remains critical for assessing the functional behavior of the valve but can be underestimated in rt-3DE imaging (Figure 5, *A*). Moreover, we were able to further distinguish this zone into its contacting and redundant sub-regions and separate these by leaflet (Figure 5, *B*). Such a level of detail is not presently possible to acquire with imaging alone and will allow us to refine our understanding of normal and regurgitant MV behavior, as well as the functional consequences of available repair techniques.

## Clinical Implications

These findings suggest that greater MV coaptation area alone may not necessarily indicate a more durable repair. These results suggest that in patients with recurrent IMR, continued LV remodeling may be the primary driving mechanism behind the regurgitation rather than the MV itself. Previous studies have extensively shown that preoperative LV dilatation and remodeling are associated with, and even predictive of, MV recurrence after URA repair.[6,27] Giammarco and colleagues[8] demonstrated in a retrospective study of patients with dilated cardiomyopathy and MR that LV ED volume was predictive of recurrence after URA repair regardless of MR etiology. Gelsomino and colleagues[4] also found that preoperative LV global remodeling played a central role in predicting recurrence, with preoperative LV ES volume as one such metric. Furthermore, they observed significant continued global LV remodeling after URA repair, which Hung and colleagues[7] showed is associated with MR recurrence. Recent analyses regarding divergent outcomes of percutaneous repair have also pointed to

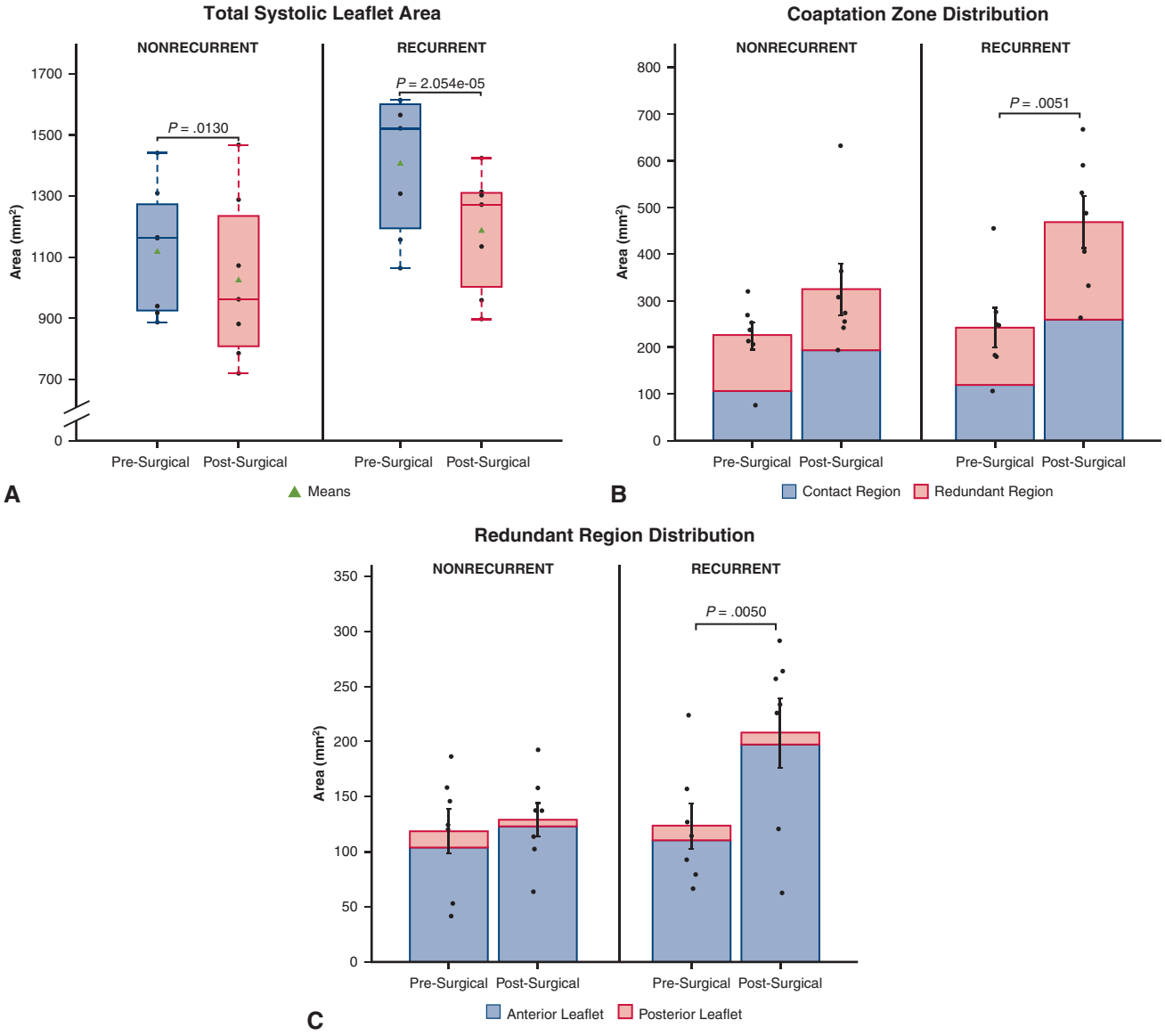


**FIGURE 6.** A, Total systolic leaflet area grouped before and after URA repair in nonrecurrent and recurrent MVs. Before surgery, the recurrent MVs are larger than the nonrecurrent MVs ($P = .0156$). B, The total coaptation zone divided into its 2 main regions—contact and redundant—for nonrecurrent and recurrent MVs, pre- and postrepair. Standard errors and significance are shown for the full coaptation zone. The coaptation zone increases significantly in recurrent MVs ($P = .0051$). C, The redundant region divided by leaflet in nonrecurrent and recurrent MVs pre- and postrepair. Standard errors and significance are shown for the full redundant region. The majority of the redundant region lies on the anterior leaflet, and the redundant region in recurrent MVs increases significantly postrepair ($P = .0050$).

the dilatation of the LV in relation to the preoperative MR grade as a possible explanation for why patients with larger LVs tend to have poorer outcomes than patients with smaller LVs but equally severe MR.[28-32] Consequently, an MV-directed treatment approach such as annuloplasty, even though it corrects the faulty coaptation behavior of the MV, may not be a durable choice in this subset of patients. Therefore, a deeper understanding is necessary regarding the functional interrelationship between the diseased LV and the MV.[33]

In addition to the remodeling of the LV, the MV leaflets themselves may have undergone more advanced adverse remodeling in patients with recurrence. Previous work has shown that presurgical strain in MV leaflets differs substantially between the nonrecurrent and recurrent patient groups, to the point that presurgical circumferential strain in the A1 segment can act as a reliable predictor of recurrence 6 months after URA repair.[22] We have also demonstrated in an ovine IMR model that MV leaflets undergo irreversible isotropic plastic deformation by 8 weeks after

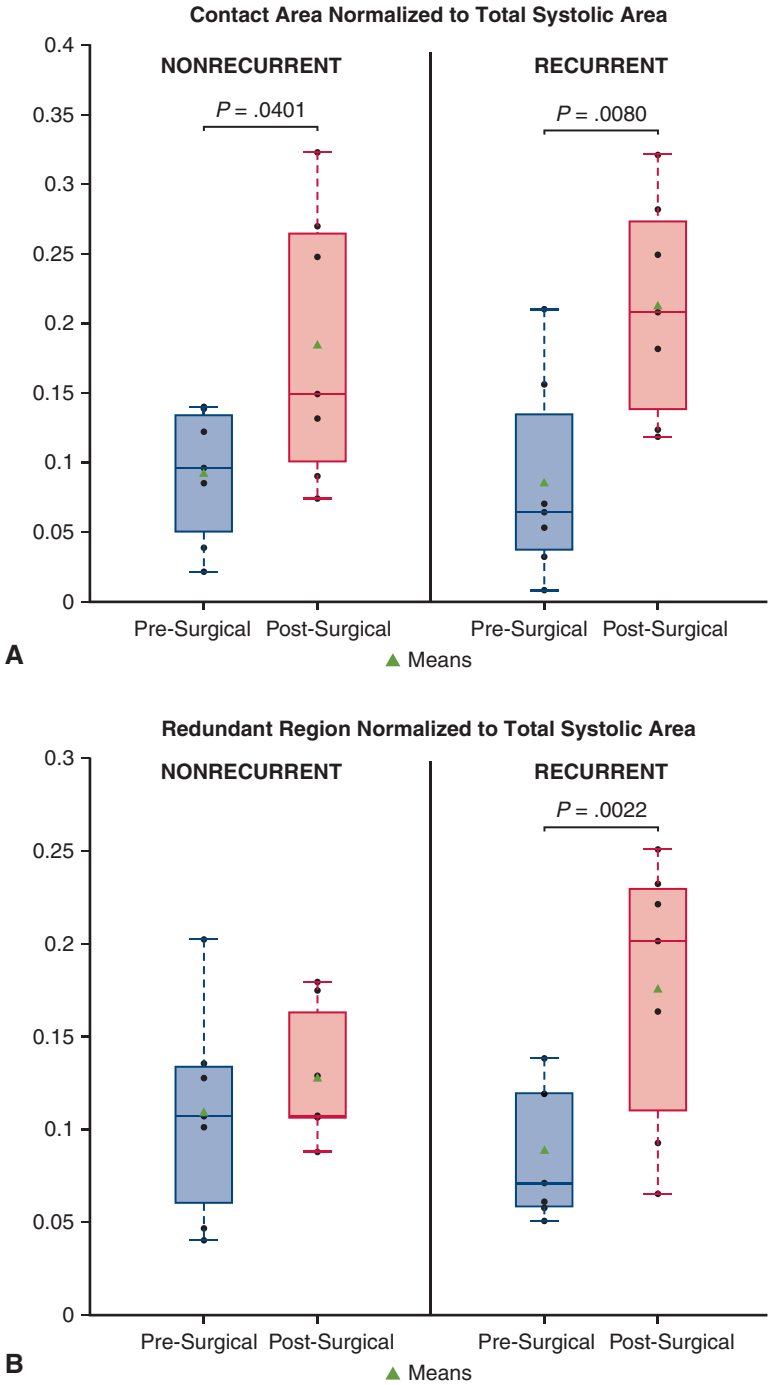


**FIGURE 7.** A, Contact region area normalized to total systolic leaflet area. While the normalized contact area increases after repair in both groups, the recurrent MVs show a greater increase ($P = .0080$, recurrent, compared with $P = .0401$, nonrecurrent). B, Redundant region area normalized to total systolic leaflet area. The normalized redundant region increases significantly in recurrent MVs, whereas in nonrecurrent MVs, it stays relatively similar.

myocardial infarction with dramatic changes in radial extensibility, and that these changes were driven by *permanent* radial distension, not damage to collagen fibers. Moreover, these tissue-level observations were associated with underlying changes in transcriptomic responses.[34-37] Therefore, methods to restore normal valve function may ultimately prove unsuccessful in patients whose MV leaflets have been plastically distorted by the disease process, and aiming to place the MV in an alternative homeostatic state may be a more sustainable option.

**TABLE 1. Computed absolute ES mitral valve tenting area and normalized mitral valve tenting area (to annular area and total systolic leaflet area) for the nonrecurrent and recurrent mitral valves before and after undersized ring annuloplasty repair**

| | | Nonrecurrent | Recurrent | *P* value |
|---|---|---|---|---|
| Presurgical | Absolute MVTa ($mm^2$) | 89.43 ± 12.55 | 157.70 ± 33.34 | .0398 |
| | Normalized MVTa (annular area) | 0.1183 ± 0.0083 | 0.1690 ± 0.0302 | .0658 |
| | Normalized MVTa (total systolic leaflet area) | 0.0789 ± 0.0072 | 0.1107 ± 0.0198 | .0997 |
| Postsurgical | Absolute MVTa ($mm^2$) | 91.83 ± 12.22 | 102.39 ± 8.71 | .2476 |
| | Normalized MVTa (annular area) | 0.2190 ± 0.0223 | 0.2488 ± 0.0215 | .1775 |
| | Normalized MVTa (total systolic leaflet area) | 0.0912 ± 0.0092 | 0.0870 ± 0.0072 | .3622 |

*MVTa*, Mitral valve tenting area.

### Study Limitations

Although we found key statistical differences in the coaptation patterns of the nonrecurrent and recurrent MVs after URA repair, our analysis was limited to 14 patients with IMR. Therefore, our findings may not reflect variations in a larger population that includes degenerative MR or mixed MR etiologies, although the same techniques can be applied to similarly study patients with other types of MR. Continued adverse LV remodeling after repair, as well as the relation between MR severity and LV size, has been shown to play a role in repair durability,[30,38-41] so future studies should be directed toward the development of an integrated LV-MV model, which will allow us to characterize the functional impact of LV pathologies on MV mechanics.

## CONCLUSIONS

The current study applied a simulation-based technique to recover the full MV geometry from clinically obtained echocardiographic images, which demonstrated that contrary to expectations, increased MV leaflet coaptation after URA repair does not necessarily indicate a more durable repair. These findings implied that in this recurrent subgroup, adverse LV remodeling, aggravated leaflet tethering, and advanced leaflet plasticity may play a larger role in the MR disease process, suggesting that MV-focused treatments alone may not lead to optimal outcomes.

### Conflict of Interest Statement

The authors reported no conflicts of interest.

The *Journal* policy requires editors and reviewers to disclose conflicts of interest and to decline handling or reviewing manuscripts for which they may have a conflict of interest. The editors and reviewers of this article have no conflicts of interest.

The authors thank Harshita Narang for assistance with the early stages of the project.

### References


1. Schubert SA, Mehaffey JH, Charles EJ, Kron IL. Mitral valve repair: the French correction versus the American correction. *Surg Clin North Am*. 2017;97:867-88.
2. McGee EC, Gillinov AM, Blackstone EH, Rajeswaran J, Cohen G, Najam F, et al. Recurrent mitral regurgitation after annuloplasty for functional ischemic mitral regurgitation. *J Thorac Cardiovasc Surg*. 2004;128:916-24.
3. Kuwahara E, Otsuji Y, Iguro Y, Ueno T, Zhu F, Mizukami N, et al. Mechanism of recurrent/persistent ischemic/functional mitral regurgitation in the chronic phase after surgical annuloplasty. *Circulation*. 2006;114(1_Suppl):I-529-34.
4. Gelsomino S, Lorusso R, Cicco GD, Capecchi I, Rostagno C, Caciolli S, et al. Five-year echocardiographic results of combined undersized mitral ring annuloplasty and coronary artery bypass grafting for chronic ischaemic mitral regurgitation. *Eur Heart J*. 2008;29:231-40.
5. Zhu F, Otsuji Y, Yotsumoto G, Yuasa T, Ueno T, Yu B, et al. Mechanism of persistent ischemic mitral regurgitation after annuloplasty. *Circulation*. 2005;112(9_Suppl):I-396-401.
6. Serri K, Bouchard D, Demers P, Coutu M, Pellerin M, Carrier M, et al. Is a good perioperative echocardiographic result predictive of durability in ischemic mitral valve repair? *J Thorac Cardiovasc Surg*. 2006;131:565-73.e2.
7. Hung J, Papakostas L, Tahta SA, Hardy BG, Bollen BA, Duran CM, et al. Mechanism of recurrent ischemic mitral regurgitation after annuloplasty. *Circulation*. 2004;110(11_Suppl_1):II-85-90.
8. Giammarco GD, Liberi R, Giancane M, Canosa C, Gallina S, Francesco AD, et al. Recurrence of functional mitral regurgitation in patients with dilated cardiomyopathy undergoing mitral valve repair: how to predict it. *Interact Cardiovasc Thorac Surg*. 2007;6:340-4.
9. Outcome after mitral valve repair for functional ischemic mitral regurgitation–PubMed. Accessed March 8, 2022. https://pubmed.ncbi.nlm.nih.gov/11858163/
10. Carpentier A, Adams DH, Filsoufi F. *Carpentier's Reconstructive Valve Surgery: From Valve Analysis to Valve Reconstruction*. Saunders/Elsevier; 2010.
11. Faletra FF, Berrebi A, Pedrazzini G, Leo LA, Paiocchi VL, Cautilli G, et al. 3D transesophageal echocardiography: a new imaging tool for assessment of mitral regurgitation and for guiding percutaneous edge-to-edge mitral valve repair. *Prog Cardiovasc Dis*. 2017;60:305-21.
12. Nielsen SL, Nygaard H, Mandrup L, Fontaine AA, Hasenkam JM, He S, et al. Mechanism of incomplete mitral leaflet coaptation—interaction of chordal restraint and changes in mitral leaflet coaptation geometry: insight from in vitro validation of the premise of force equilibrium. *J Biomech Eng*. 2002;124:596-608.
13. Guo Y, He Y, Zhang Y, Ge S, Sun L, Liu W, et al. Assessment of the mitral valve coaptation zone with 2D and 3D transesophageal echocardiography before and after mitral valve repair. *J Thorac Dis*. 2018;10:283-90.
14. Yamada R, Watanabe N, Kume T, Tsukiji M, Kawamoto T, Neishi Y, et al. Quantitative measurement of mitral valve coaptation in functional mitral regurgitation: in vivo experimental study by real-time three-dimensional echocardiography. *J Cardiol*. 2009;53:94-101.
15. Yamauchi T, Taniguchi K, Kuki S, Masai T, Noro M, Nishino M, et al. Evaluation of the mitral valve leaflet morphology after mitral valve reconstruction with a concept "coaptation length index.". *J Cardiac Surg*. 2005;20:432-5.

16. Bouma W, Aoki C, Vergnat M, Pouch AM, Sprinkle SR, Gillespie MJ, et al. Saddle-shaped annuloplasty improves leaflet coaptation in repair for ischemic mitral regurgitation. *Ann Thorac Surg*. 2015;100:1360-6.
17. Cobey FC, Swaminathan M, Phillips-Bute B, Hyca M, Glower DD, Douglas PS, et al. Quantitative assessment of mitral valve coaptation using three-dimensional transesophageal echocardiography. *Ann Thorac Surg*. 2014;97:1998-2004.
18. Shudo Y, Matsue H, Toda K, Hata H, Fujita S, Taniguchi K, et al. A simplified echocardiographic measurements of direct effects of restrictive annuloplasty on mitral valve geometry. *Echocardiography*. 2010;27:931-6.
19. Maisano F, Falk V, Borger MA, Vanermen H, Alfieri O, Seeburger J, et al. Improving mitral valve coaptation with adjustable rings: outcomes from a European multicentre feasibility study with a new-generation adjustable annuloplasty ring system. *Eur J Cardiothorac Surg*. 2013;44:913-8.
20. Gogoladze G, Dellis SL, Donnino R, Ribakove G, Greenhouse DG, Galloway A, et al. Analysis of the mitral coaptation zone in normal and functional regurgitant valves. *Ann Thorac Surg*. 2010;89:1158-61.
21. Rego BV, Khalighi AH, Drach A, Lai EK, Pouch AM, Gorman RC, et al. A noninvasive method for the determination of in vivo mitral valve leaflet strains. *Int J Numer Meth Bio*. 2018;34:e3142.
22. Narang H, Rego BV, Khalighi AH, Aly A, Pouch AM, Gorman RC, et al. Pre-surgical prediction of ischemic mitral regurgitation recurrence using in vivo mitral valve leaflet strains. *Ann Biomed Eng*. 2021;49:3711-23.
23. Bouma W, Lai EK, Levack MM, Shang EK, Pouch AM, Eperjesi TJ, et al. Preoperative three-dimensional valve analysis predicts recurrent ischemic mitral regurgitation after mitral annuloplasty. *Ann Thorac Surg*. 2016;101:567-75.
24. Drach A, Khalighi AH, Sacks MS. A comprehensive pipeline for multi-resolution modeling of the mitral valve: validation, computational efficiency, and predictive capability. *Int J Numer Method Biomed Eng*. 2018;34:e2921.
25. Otto CM, Nishimura RA, Bonow RO, Carabello BA, Erwin JP III, Gentile F, et al. 2020 ACC/AHA guideline for the management of patients with valvular heart disease: a report of the American College of Cardiology/American Heart Association Joint Committee on clinical practice guidelines. *Circulation*. 2021;143:e72-227.
26. von Stumm M, Dudde F, Holst T, Sequeira-Gross T, Pausch J, Müller L, et al. Predicting clinical outcome by indexed mitral valve tenting in functional mitral valve regurgitation. *Open Heart*. 2021;8:e001483.
27. Braun J, Bax JJ, Versteegh MIM, Voigt PG, Holman ER, Klautz RJM, et al. Preoperative left ventricular dimensions predict reverse remodeling following restrictive mitral annuloplasty in ischemic mitral regurgitation. *Eur J Cardiothorac Surg*. 2005;27:847-53.
28. Obadia JF, Messika-Zeitoun D, Leurent G, Iung B, Bonnet G, Piriou N, et al. Percutaneous repair or medical treatment for secondary mitral regurgitation. *N Engl J Med*. 2018;379:2297-306.
29. Stone GW, Lindenfeld J, Abraham WT, Kar S, Lim DS, Mishell JM, et al. Transcatheter mitral-valve repair in patients with heart failure. *N Engl J Med*. 2018; 379:2307-18.
30. Grayburn PA, Sannino A, Packer M. Proportionate and disproportionate functional mitral regurgitation a new conceptual framework that reconciles the results of the MITRA-FR and COAPT Trials. *JACC Cardiovasc Imaging*. 2018;12: 353-62.
31. Stolfo D, Luca AD, Morea G, Merlo M, Vitrella G, Caiffa T, et al. Predicting device failure after percutaneous repair of functional mitral regurgitation in advanced heart failure: implications for patient selection. *Int J Cardiol*. 2018; 257:182-7.
32. Packer M, Grayburn PA. Contrasting effects of pharmacological, procedural, and surgical interventions on proportionate and disproportionate functional mitral regurgitation in chronic heart failure. *Circulation*. 2019; 140:779-89.
33. Liu H, Narang H, Gorman R, Gorman J, Sacks MS. Functional imaging and modeling of the heart, 11th International Conference, FIMH 2021, Stanford, CA, USA, June 21-25, 2021, proceedings. *Lect Notes Comput Sci*. 2021; 12738:425-34.
34. Howsmon DP, Rego BV, Castillero E, Ayoub S, Khalighi AH, Gorman RC, et al. Mitral valve leaflet response to ischaemic mitral regurgitation: from gene expression to tissue remodelling. *J Roy Soc Interface*. 2020;17:20200098.
35. Sacks M, Drach A, Lee CH, Khalighi A, Rego B, Zhang W, et al. On the simulation of mitral valve function in health, disease, and treatment. *J Biomechanical Eng*. 2019;141:0708041-07080422.
36. Rego BV. Remodeling of the mitral valve: an integrated approach for predicting long-term outcomes in disease and repair, *Ph.D. thesis*. The University of Texas at Austin; 2019.
37. Rego BV, Khalighi AH, Gorman JH, Gorman RC, Sacks MS. Simulation of mitral valve plasticity in response to myocardial infarction. *Ann Biomed Eng*. 2022;1-17.
38. Grayburn PA, Sannino A, Packer M. Distinguishing proportionate and disproportionate subtypes in functional mitral regurgitation and left ventricular systolic dysfunction. *JACC Cardiovasc Imaging*. 2020;14:726-9.
39. Salvatore T, Ricci F, Dangas GD, Rana BS, Ceriello L, Testa L, et al. Selection of the optimal candidate to mitraclip for secondary mitral regurgitation: beyond mitral valve morphology. *Front Cardiovasc Med*. 2021;8:585415.
40. Serratore S, Polimeni A, Mongiardo A, Spaccarotella C, Sorrentino S, Panuccio G, et al. 812 Prognostic impact of the COAPT inclusion and exclusion criteria in real-world patients with secondary mitral regurgitation undergoing MitraClip implantation. *Eur Heart J Suppl*. 2021;23(Suppl_G). suab149.006.
41. Sugiura A, Kavsur R, Spieker M, Iliadis C, Goto T, Öztürk C, et al. Recurrent mitral regurgitation after MitraClip: predictive factors, morphology, and clinical implication. *Circ Cardiovasc Interv*. 2021;15:e010895.

**Key Words:** mitral valve imaging, mitral valve mechanics, mitral valve regurgitation, mitral valve repair, myocardial infarction